Materials Today Communications 34 (2023) 105244

Contents lists available at ScienceDirect

Materials Today Communications

journal homepage: www.elsevier.com/locate/mtcomm

Gas metal arc welding with undermatched filler wire for hot-press-formed steel of 2.0 GPa strength: Influence of filler wire strength and bead geometry

Dong-Yoon Kim [a,b], Tae Hyen Lee [a,c], Cheolhee Kim [a,d], Minjung Kang [a,*], Junhong Park [b,*]

[a] Advanced Joining & Additive Manufacturing R&D Department, Korea Institute of Industrial Technology, Incheon 21999, South Korea
[b] Department of Mechanical Convergence Engineering, Hanyang University, Seoul 04763, South Korea
[c] Department of Mechanical Design Engineering, Hanyang University, Seoul 04763, South Korea
[d] Department of Mechanical and Materials Engineering, Portland State University, OR 97207, USA

ARTICLE INFO

Keywords:
Hot press forming steel
Gas metal arc welding
Filler wire strength
Lap joint
Throat thickness
Leg length

ABSTRACT

Commercial welding filler wires have less strength than hot-press-forming (HPF) steels. As the 2.0 GPa-HPF steel sheets have been released, their lap welding characteristics were investigated using gas metal arc welding in this study. The base metal was 1.1 mm-thick 2.0 GPa-HPF steel sheets, and three filler metal wires considered in this study (W540, W920, and W980) had tensile strengths of 540, 920, and 980 MPa, respectively. Gas metal arc welding was performed under a controlled short-circuit mode, and the wire feed speed (WFS) was selected as a process parameter. Tensile-shear test and microscopy were performed to evaluate the joint strength and metallurgical characteristics. The joint strength increased when WFS increased. When the WFS was 6 m/min or higher and high strength filler wires were applied to it, a heat affected zone (HAZ) fracture was observed in the tensile-shear test, with a tensile strength of approximately 1150 MPa. The fracture location was the boundary of the sub-critical HAZ (comprising tempered martensite) and intercritical HAZ (comprising polygonal ferrite and martensite). The weld metal (WM) hardness for W540 welds was 270 HV, and that for W920 and W980 was 414–419 HV, while the joint strength for the WM fracture was proportional to the throat thickness. For low WFS (when the heat input per unit length and welding current were low), high strength filler metals enhanced the joint strength, while high welding currents and deep penetration welding modes were recommended for W540. This study provided the filler wire and bead geometry design for the lap welds of 2.0 GPa HPF steel sheets.

1. Introduction

Hot-press-forming (HPF) steels have been used in crashworthy automotive systems, such as anti-collision beams, bumpers, and b-pillar reinforcements, to protect passengers from crashes [1]. Owing to its ultimate tensile strength of more than 1.5 GPa, energy efficiency and emission reduction demands are achieved without losing collision safety [2]. Recently, steelmakers have released novel HPF steels that exhibit an ultimate tensile strength of over 2.0 GPa, obtained by coupling alloy designs and hot stamping [2–5].

Welding is an essential assembly process in manufacturing automotive parts. Since HPF steel has a fully martensitic microstructure that is sensitive to heat input, the heat affected zone (HAZ) is softened during welding when relatively soft tempered martensite is formed [6–9]. During welding martensite-based ultra-high-strength steel (UHSS), HAZ softening is unavoidable. Hence, a relatively low heat input process is preferred to minimize the size and magnitude of HAZ softening [6,10]. Generally, the joint efficiency of weld connections is defined as the ratio of the weld metal's (WM) strength to that of the base metal (BM) or HAZ.

In resistance spot and laser overlap welding on UHSS, the area of joint interface and HAZ softening determined the joint efficiency. Zhu et al. performed resistance spot welding on 2.0 GPa-HPF steel and reported that pull-out failure occurred when a weld nugget size was 5 times higher than the square root of the sheet's thickness [11]. Lu et al. [2] investigated the laser weldability of 2.0 GPa-HPF steels using a butt joint and achieved a fracture strength of 1.5 GPa in HAZ failure cases. They reported that the softened HAZ increased with the heat input. Kim et al. [6] also showed that the laser-butt-welded 2.0 GPa-steel had a

* Corresponding authors.
E-mail addresses: kmj1415@kitech.re.kr (M. Kang), parkj@hanyang.ac.kr (J. Park).

https://doi.org/10.1016/j.mtcomm.2022.105244
Received 5 October 2022; Received in revised form 27 November 2022; Accepted 21 December 2022
Available online 24 December 2022

Table 1
Chemical composition of the base metal (wt%).

Chemical composition							
C	Si	Mn	P	S	Cr	Ni	Mo
0.346	0.25	1.29	0.011	0.001	0.14	0.04	0.02
V	Ti	Cu	Al	Nb	B	N	Fe
0.01	0.01	0.00	0.033	0.044	0.0015	0.003	Bal.

softened HAZ and tensile test specimen fracture at the boundary between the subcritical HAZ (SCHAZ) and intercritical HAZ (ICHAZ), which had the lowest hardness. Kim et al. [12] and Kang et al. [13] performed laser overlap welding on 2.0 GPa-HPF steels and achieved an equivalent tensile-shear strength of 810 MPa and 1 GPa using a multi-mode laser and a single mode laser, respectively.

Contrarily, in gas metal arc welding (GMAW), the joint efficiency was influenced by the shape of welded joints and filler metal strength [14,15]. For instance, in fillet joints, the leg length and throat thickness are representative of joint characteristics among the weld features for load carrying. Additionally to weld geometry, high joint efficiency can be achieved by using high-strength filler wires [9,16]. These filler wires are selected to satisfy the weld strength and toughness [3,17]. High-strength welding filler wires have been developed for heavy industries, while commercial products with a tensile strength of 980 MPa or higher are available in the market. Recently, higher grade welding filler wires have been introduced. Haslberger et al. developed a filler wire with a minimum yield strength of 1100 MPa [4,18], while Holly et al. presented a new metal-cored wire with a tensile strength of 1150 MPa.

While high-strength filler wires have been applied in heavy industries, conventional filler wires, such as AWS ER70s, with lower strengths than BM have widely been applied on UHSS in automotive industries [19]. The major difference between both applications is the joint type. In heavy industries, butt and fillet joints are mainly used to assemble relatively thick BM, while lap joints are preferred in thin BM sheets in automotive industries. During the gas metal arc welding of lap-jointed martensitic steel sheets with strengths of 1.5 GPa, conventional filler wires (AWS ER70S) with tensile strengths of 500 MPa cause HAZ fractures in the tensile shear test by selecting appropriate welding parameters [20]. However, only one research result for autogenous butt welding is currently available for 2.0 GPa-HPF steels [21]. To date, arc welding using filler metals has not been evaluated, and the influence of filler metals on joint strength still remains unknown.

This research aims to elucidate how the strength of filler wires contribute to the tensile shear strength of lap-welded 2.0 GPa-UHSS. Three types of filler wires with tensile strengths of 540, 940, and 980 MPa were used for GMAW. The short-circuiting droplet transfer mode for GMAW was selected to minimize the HAZ width. This study provides guidelines for selecting a suitable filler wire and weld geometry for 2.0 GPa-UHSS steel lap joints.

2. Experiments

The base material was a 1.1 mm-thick boron-alloyed steel, Docol® PHS CR 2000, and was supplied by SAAB AB. The specimens were prepared using the HPF process. They were heated for 5 min in a furnace at 950 °C to complete the austenitic phase transformation and later quenched in a water-cooled die where the temperature was maintained at 25 °C. After the HPF, the tensile strength and hardness achieved an average value of 2.08 GPa and 609 HV, respectively [22]. The specimens were machined to 150 mm × 120 mm, and the specimen surface was milled to eliminate the oxide scales generated during the HPF process. The chemical compositions of the materials were analyzed using an optical emission spectrometer (Table 1).

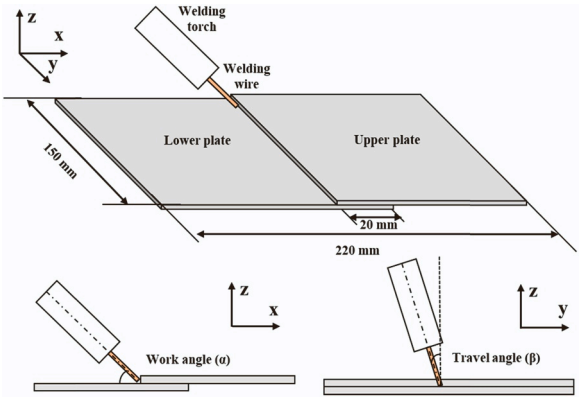

Fig. 1. Schematic of welding joint preparation.

Three types of filler wires with different tensile strengths were prepared to assess the mechanical properties of the weld joints. In this study, AWS A5.18 ER70S-3, AWS A5.28 ER110S-G, and AWS A5.28 ER120S-G are referred to as W540, W920, and W980, respectively. The chemical compositions and mechanical properties of the applied filler wires, which were provided by manufacturers, are listed in Table 2. Each filler wire had a diameter of 1.0 mm.

A short-circuit mode arc welding power source (CMT 4000 Advanced, Fronius, Wels, Austria) was used for the lap fillet joint welding. The power source had a specialized short-circuit mode called cold metal transfer (CMT), which was characterized by low heat input, spatter-free metal transfer, excellent gap-bridging ability, and elegant bead formation [23]. Specimens were overlapped with a length of 20 mm (Fig. 1). The distance between the contact tip and workpiece was maintained at 15 mm, and a 90 % Ar + 10 % CO_2 mixed shielding gas was provided with a flow rate of 20 L/min. A push-travel technique was employed with an angle of 20°, and the work angle was set to 45°. The wire feeding speed (WFS) was chosen as the process variable (Table 3). The WFS increased from 4.0 m/min to 8.0 m/min within 1.0 m/min. The average welding current/voltage was changed from 99 A/10.7 V to 190 A/18.8 V according to the WFS.

Three tensile shear test specimens were extracted from the welded specimen (Fig. 2) and machined according to the ASTM E8M standard (Fig. 3). The tensile-shear test was conducted using a universal material testing machine (Shimadzu, Kyoto, Japan) with a maximum load of 294 kN. A spacer has been installed to prevent rotation of the specimen, and the head speed was 5 mm/min in the test. Vickers hardness profiles were measured on the transverse section with an indent spacing, load, and holding time of 200 μm, 1.96 N, and 10 s, respectively, according to the ASTM E384–99 standard. During welding, the current and voltage waveforms were measured using a data acquisition system (NI 9229 module) with a sampling frequency of 50 kHz. After welding, cross-sectional images were prepared to analyze the weld throat, leg length,

Table 2
Chemical composition and mechanical properties of used filler wires.

	Chemical composition (wt%)						Mechanical properties		
	C	Si	Mn	Cr	Mo	Ni	Tensile strength (MPa)	Yield strength (MPa)	Elongation (%)
W540	0.07	0.83	1.48	–	–	–	540	430	28
W920	0.07	0.70	1.60	0.3	0.5	1.75	927	810	16
W980	0.12	0.80	1.90	0.45	0.55	2.35	980	930	14

Table 3
Welding conditions used in the experiment.

Parameters	Value
Power source	CMT Advanced 4000, Fronius
Wire feeding speed (m/min)	4.0–8.0 (interval of 1.0)
Welding speed (cm/min)	120
Work angle (α*, °)	45
Travel angle (β*, °)	20
Contact tip to workpiece distance (mm)	15
Shielding gas, flow rate (L/min)	90 % Ar-10 % CO_2, 20

Note) * marked in Fig. 1.

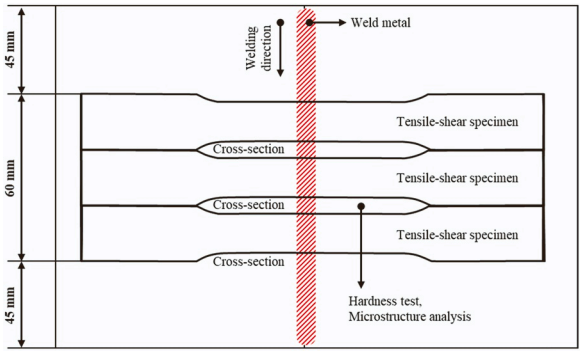

Fig. 2. Configuration of test-specimens.

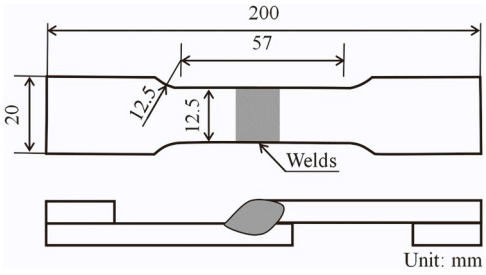

Fig. 3. Configuration of tensile-shear test specimen.

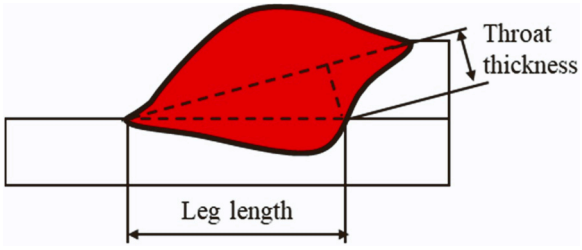

Fig. 4. Schematic of joint features.

and microstructures. These specimens were polished and etched with a 3 % natal solution containing 3 and 100 ml of HNO_3 and H_2O, respectively. As shown in Fig. 4, the weld size (throat thickness and leg length), which affects tensile-shear strength, was measured using optical microscopy. The microstructures of the welds were observed using field-emission scanning electron microscopy (FE-SEM) (Thermo Fisher Scientific, Waltham, MA, USA).

3. Results

3.1. Process stability

Two high strength filler wires (W920 and W980) showed process stability, which was similar to the conventional filler wire (W540). Consistent bead widths were maintained for all the filler wires, while wire feeding and spatter generation issues were absent in the experiment.

As a quantitative measure of the arc and metal transfer, current and voltage waveforms were recorded, while notable differences among the wires were not observed (Fig. 5). For example, when the WFS was 5 and 7 m/min, the difference in the period and peak current time among the wires was between 0.98 and 0.06 ms, respectively. The standard deviation of the period and peak current was less than 3.57 % and 3.50 %, respectively. The peak current value was exactly similar for all the wires, and its standard deviation was less than 0.8 % of the average peak current (Table 4).

3.2. Weld geometry

Geometric imperfection from the bead appearance, such as overlap and undercut, was not identified for all welding conditions. Weld defects in the cross-section, such as porosity and cracking, were not observed (Fig. 6).

In low WFSs, weld bead surfaces for high strength filler wires were more convex than those for W540, which increased the toe angle and decreased the fatigue strength. Since the bead convexity is influenced by the wetting between materials, high alloying contents in high strength wires was one of the causes of bead convexity. By increasing the WFS (the heat input), the bead convexity became similar for all the wires.

The weld size feature of the leg length and throat thickness varied according to the WFS and wire (Fig. 7). The throat thickness and leg length increased with an increase in WFS. The relationship between the weld size and wire was not clear in this experiment. The maximum differences between the throat thickness and leg length at the fixed WFS was 0.07 mm at a WFS of 6.0 and 0.94 mm at a WFS of 4.0 m/min, respectively. The alloying elements influenced the bead shapes by varying the free surface profiles, the thermal diffusivity of WM, and weld pool flow owing to the Marangoni flow and buoyancy.

3.3. Microstructure and hardness profile

The microstructure of weldment, except WM, was similar for all the wires, and the BM and HAZ microstructures for a WFS of 7 m/min is shown in Fig. 8. The BM was fully martensitic because it was quenched in a water-cooled die during the HPF process (Fig. 8a). In the SCHAZ where the peak temperature was less than the Ac1 temperature, tempered martensite was observed owing to carbide precipitation (Fig. 8b). In the ICHAZ where the peak temperature was between Ac1 and Ac3 temperatures, a dual phase of austenite and ferrite was formed in the peak temperature. The austenite region was transformed into martensite during cooling, while the ferrite region remained unchanged (Fig. 8c). At the boundary of the ICHAZ and fine grain HAZ (FGHAZ) where the peak temperature was below the Ac3 temperature, small amounts of polygonal ferrite were found in almost fully martensitic structures (Fig. 8d). In FGHAZ and coarse grain HAZ (CGHAZ) where the peak temperature was between the Ac3 and melting temperatures, full martensite was formed owing to the full austenization during heating and rapid cooling, while the grain size of FGHAZ was slightly smaller than that of CGHAZ. Cooling rates from 800 to 500 °C were 70 K/s according to the calculation based on the analytic solution for temperature distribution in arc welding. The details of the calculation were presented in the previous study [21]. The cooling rate was higher than 50 K/s, and was recommended for the full martensite formation by the manufacturer [24].

The microstructure of WM was determined by the cooling rate and dilution of filler metals and BMs. The WM of W540 comprised predominately acicular ferrite and a small fraction of bainite (Fig. 9). Grain boundary ferrite was also clearly observed, while Widmanstätten ferrite was hardly observed. In the WM of W920, the fraction of bainite was elevated, while the size of acicular ferrite was reduced compared to that

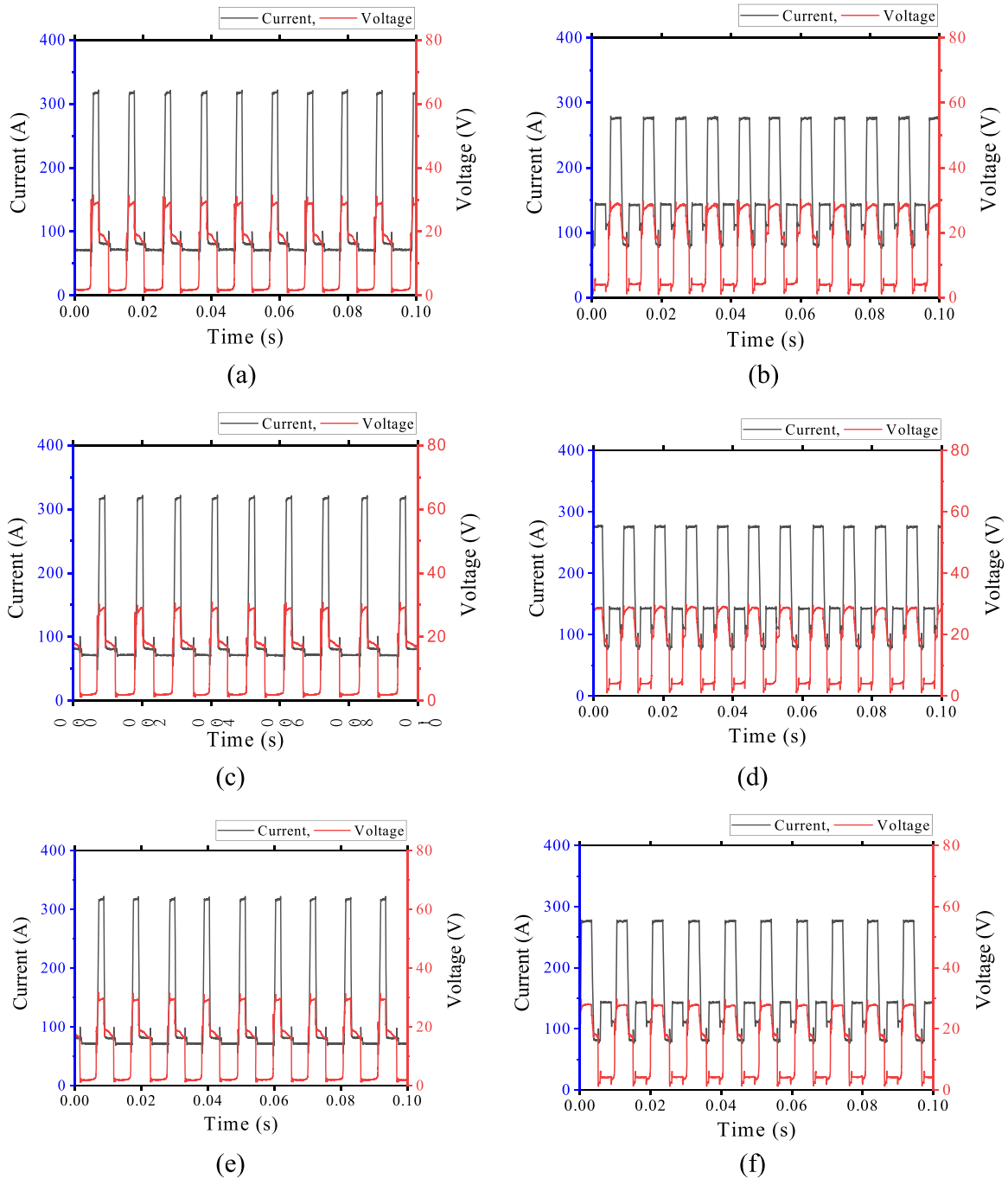

Fig. 5. Waveform analysis results according to filler wire and WFS: a) W540, 5.0 m/min; b) W540, WFS 7.0 m/min; c) W920, 5.0 m/min; d) W920, 7.0 m/min; e) W980, 5.0 m/min; and f) W980, 7.0 m/min.

Table 4
Measured welding current waveform characteristics.

WFS (m/min)	Filler wire	Period (ms)		Peak current time (ms)		Peak current (A)	
		Average	Standard deviation	Average	Standard deviation	Average	Standard deviation
5	W540	10.47	0.26	1.43	0.05	317	1.11
	W920	10.89	0.20	1.45	0.03	317	1.08
	W980	10.59	0.18	1.49	0.01	317	1.22
7	W540	9.24	0.33	2.83	0.03	276	0.97
	W920	9.15	0.16	2.85	0.02	276	2.21
	W980	10.13	0.12	2.87	0.01	276	0.92

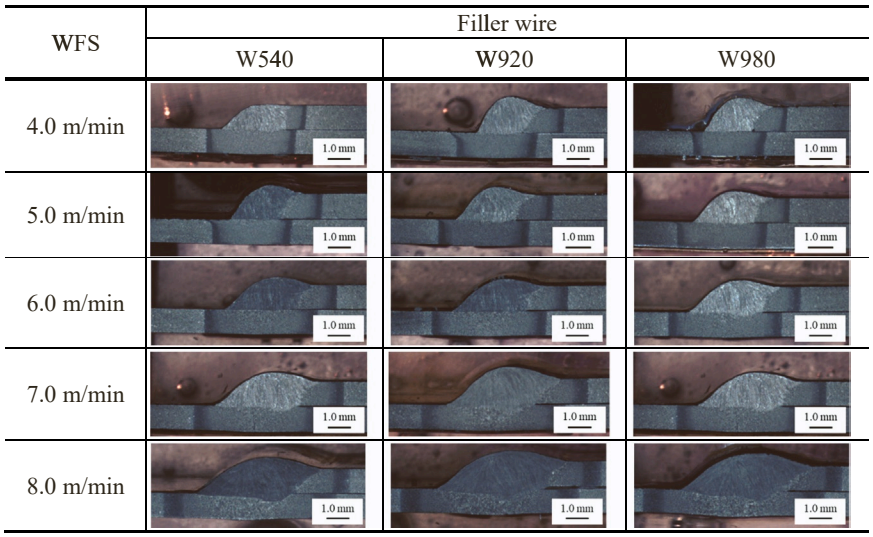

Fig. 6. Cross-sectional images of GMAW welds depending on filler wires and WFS.

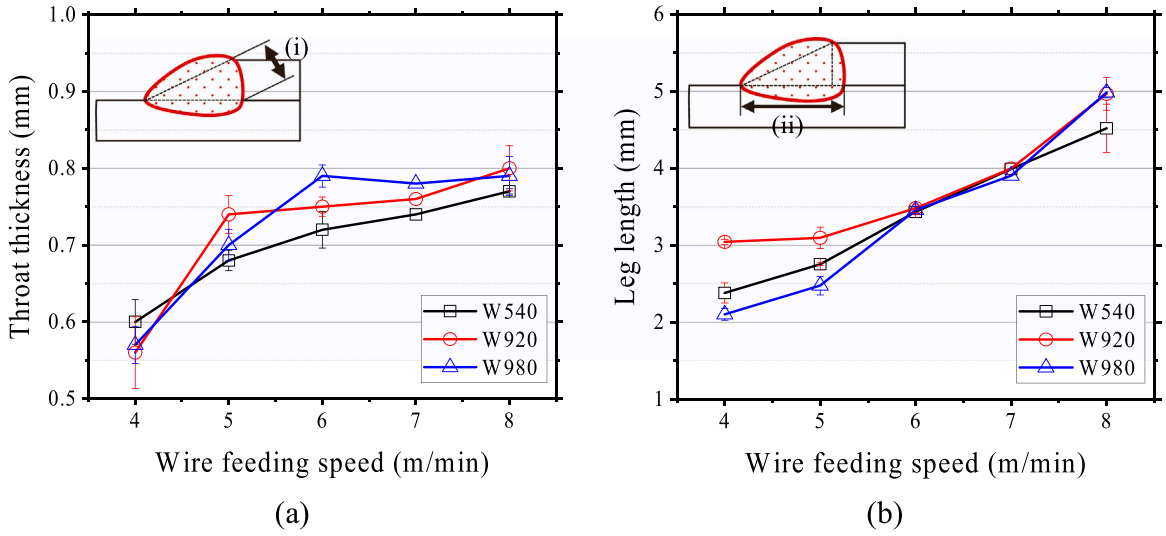

Fig. 7. Measured weld size of: a) throat thickness and b) leg length.

of W540. The WM of W980 also comprised bainite and lath-like martensite. The microstructure formations were similar to those reported by John et al. [8]. Polygonal ferrite was hard to find in the WM of W920 and W980 owing to high alloying elements, such as carbon and manganese.

The hardness in the SCHAZ decreased from the BM to the ICHAZ, which was caused by the tempering of martensite (Fig. 10). The softening owing to tempered martensite was the highest at the boundary between the SCHAZ and ICHAZ, while the hardness within the ICHAZ increased. In the FGHAZ and CGHAZ, the hardness was saturated owing to the full martensitic microstructure, which later decreased in the WM owing to the dilution of the filler metal. The hardness profiles coincided well with the microstructure in Figs. 8 and 9. In the WM of W540 weldment, the hardness was about 2/3 of that of W980 weldment. It had the lowest hardness because it was constituted of ferrite and bainite, while other locations contained, fully or partially, martensite and tempered martensite.

3.4. Tensile-shear test

The fracture load in the tensile-shear test increased by increasing the WFS (Fig. 11). In Fig. 11, the equivalent tensile stress was calculated by dividing the fracture load by the specimen cross-sectional area. Regarding high strength steel wires, the HAZ fracture was accomplished when the WFS was 6 m/min or higher. The tensile strength was approximately 1150 MPa for all HAZ fracture cases. Regarding the conventional wire (W540), all the specimens were fractured at the WM, although the fracture load increased with the WFS. At the fixed WFS, high strength steel wires showed higher fracture loads than that of W540, which originated from lower WM strengths. In the HAZ fracture mode, the filler wires did not affect the fracture load. However, the heat input affected the HAZ softening and fracture load.

Regarding WM fractures, the fracture was initiated at the root and propagated into the upper sheet (Fig. 12a). Regarding HAZ fractures, the fracture was initiated in the middle of the boundary plane of SCHAZ and ICHAZ and propagated into the edges, while the shear lip was on the edges of the lower sheet (Fig. 12b).

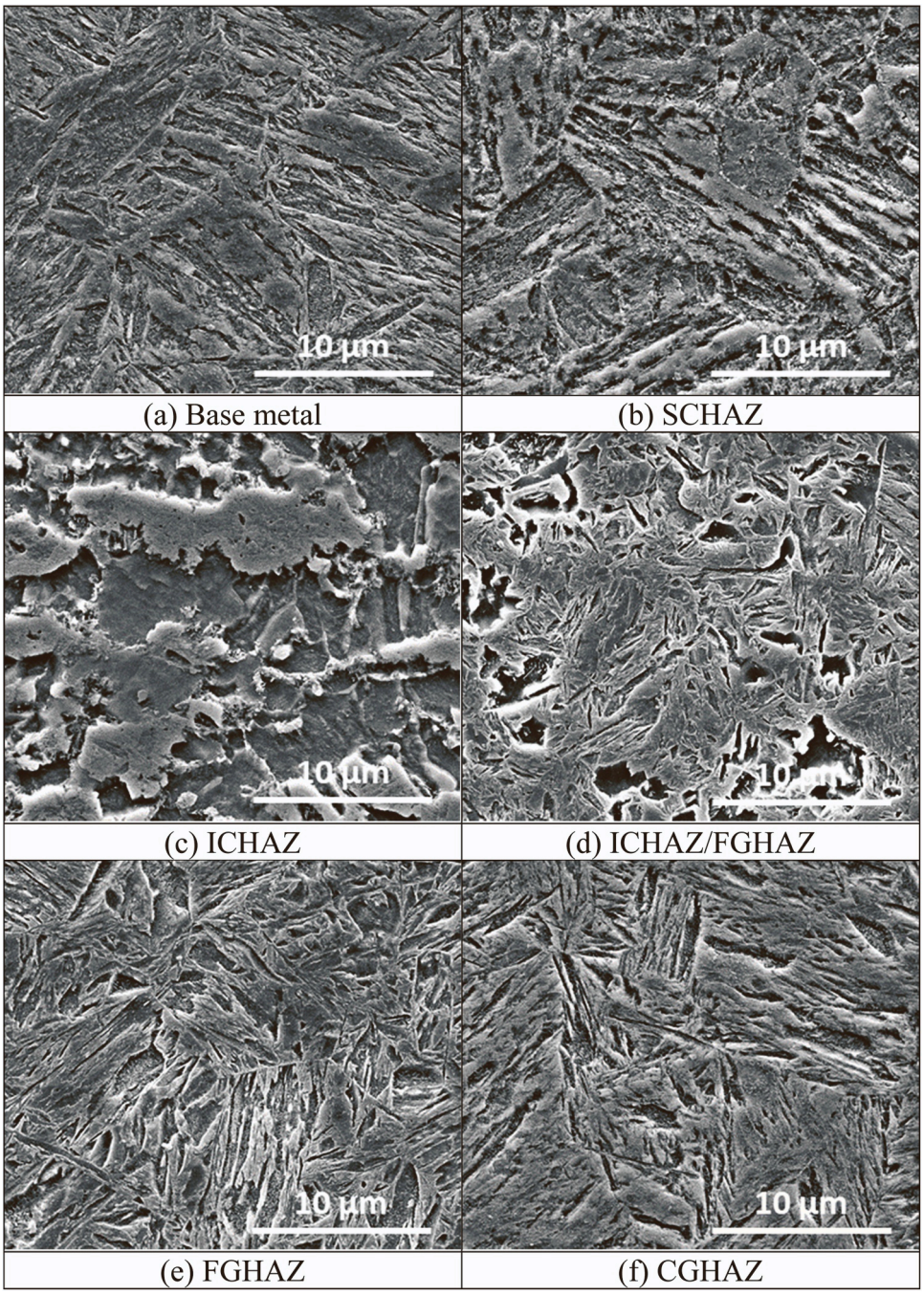

Fig. 8. SEM images of HAZ (WFS: 7 m/min): a) base metal; b) SCHAZ; c) ICHAZ; d) ICHAZ/FGHAZ; e) FGHAZ; and f) CGHAZ.

4. Discussion

The conventional filler wire (W540) and high strength filler wires (W920 and W980) were applied during the lap welding of 2.0 GPa HPF steel sheets to investigate the relationship between the filler metal and joint strength.

The filler wires had a diameter of 1.0 mm, and the process stability was confirmed for all wires in terms of the bead consistency, stability in arc and metal transfer, and bead appearance and cross-sectional shape. The tempered martensite in the SCHAZ and partial ferritic phase in the ICHAZ caused HAZ softening, which is common during the welding of martensite strengthened steels. The minimum hardness was identified at the boundary of the SCHAZ and ICHAZ, which coincided with the nanoindentation hardness measurement in previous studies [22]. The heat input per unit length in this study ranged from 0.54 kJ/cm to 1.74 kJ/cm, and the minimum hardness was 320 HV. It was approximately 80 MPa lower than that during laser welding trials, which had a heat input per unit length ranging from 0.15 kJ/cm to 0.2 kJ/cm [22]. The higher heat input during arc welding was caused by the polygonal ferrite formation in the ICHAZ, while the plate-like or acicular ferrite formation was identified in the ICHAZ of laser welds [13,22,25]. The morphology according to the heating rate was explained by Apple and Krauss [26]. During tensile testing, the maximum fracture load was achieved in the HAZ fracture mode, and the average tensile strength in the HAZ fracture load was 1150 MPa. The maximum load carrying capacity of the lap joint welds was determined by the minimum hardness

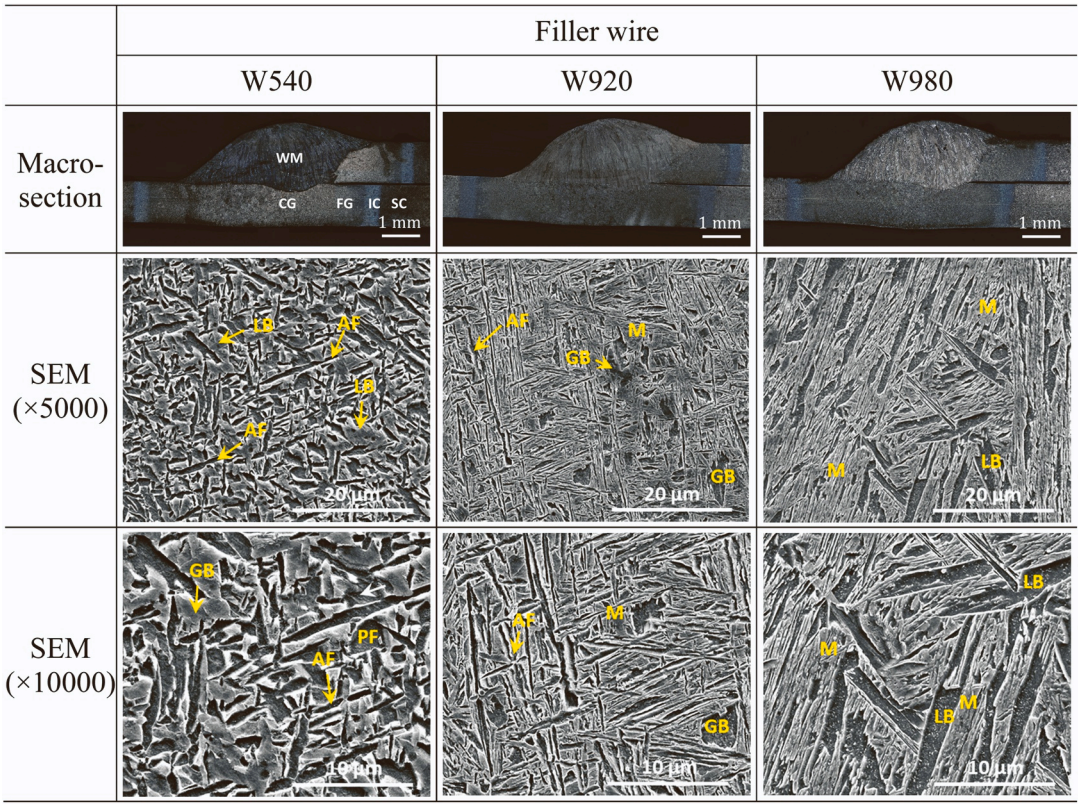

Fig. 9. SEM images of WM (WFS: 7 m/min) (PF–polygonal ferrite, AF–acicular ferrite, GB–granular bainite, LB–lower bainite, M–martensite).

of HAZ.

The filler metal strength and weld geometry determined the fracture mode and load in the WM fracture mode. In this study, the filler metal strength was lower than that of the BM. Hence, the fracture location was either the WM or HAZ. The WM for high strength filler wires comprised martensite and bainite. It was harder than softened HAZ, which comprised martensite and polygonal ferrite. The WM for low strength filler wires comprised bainite and ferrite, with hardness of 270 MPa and was the lowest among the microstructures in this study. In addition to the WM strength, weld geometry is an important factor in determining the load carrying capacity of WMs. The leg length and throat thickness affected the joint strength, and their relationship to the joint strength was redrawn, as shown in Figs. 7 and 11. The linear relationship was more obvious in the throat thickness and joint strength (Fig. 13). The correlation coefficients for W540, W920, and W980 wires were 0.94, 0.95, and 0.98, respectively. For W920 and W980 wires, when the throat thickness was over 0.75 mm and the leg length was over 3.5 mm, the HAZ fracture was achieved. However, the joint strength for W540 wire increased with the throat thickness and leg length, while the WM fracture was identified under all the conditions.

When the WFS was 5 m/min or less, high strength filler wires (W920 and W980) ensured a higher joint strength than the conventional wire (W540). Under the aforementioned conditions, the WM factures occurred and the strength was determined by the WM strength and throat thickness. Notably, the maximum throat thickness for W540 wire was 0.77 mm in this study, which was enhanced by higher WFS or weld modes other than CMT for deep penetration. Higher WFS is accompanied by higher welding current. The thickness of the BM was 1.1 mm. Hence, higher throat thickness was feasible without weld defects. The maximum average welding current in this study was 190 A, which had a margin to the spray transition current of 250 A [27]. However, higher WFS is also accompanied by higher heat inputs. Hence, thermal distortion can increase. The penetration in the CMT mode was relatively low compared to the standard mode (the constant voltage mode) and pulsed mode. So the standard and pulse mode welding can enhance the penetration. Further, the pulsed CMT mode enabled advantages from both the CMT and pulsed mode [28]. In the previous study on 1.5 GPa-martensitic steel [20], the HAZ fracture was achieved in the standard and pulsed modes.

5. Conclusion

This study is the first investigation on the lap joint welding of 2.0 GPa-HPF steel using GMAW, whereby the effects of the filler wire strength on the joint strength and metallurgical characteristics was exhibited. The conventional low strength (W540) and two high strength filler wires (W920 and W980) were selected as the filler metals. The following conclusions were derived:

1. Sound welds without weld imperfection were established for all the filler wires and WFSs. During the tensile-shear testing, the specimens were fractured either at the WM or HAZ, and the maximum load carrying capacity was determined by HAZ softening. Regarding the heat input range of 0.540 kJ/cm to 1,74 kJ/cm, the maximum tensile strength was 1150 MPa, and the fracture location was the boundary between the SCHAZ and ICHAZ.
2. The load carrying capacity of WM was related to the strength of FM and weld geometric attributes. In the WM facture mode, the joint strength increased by increasing the WFS. When the WFS was 6 m/min or higher for W920 and W960 wires, the facture mode changed to the HAZ fracture, while the facture mode for W540 wire was the WM fracture for all the conditions. Among the weld geometric

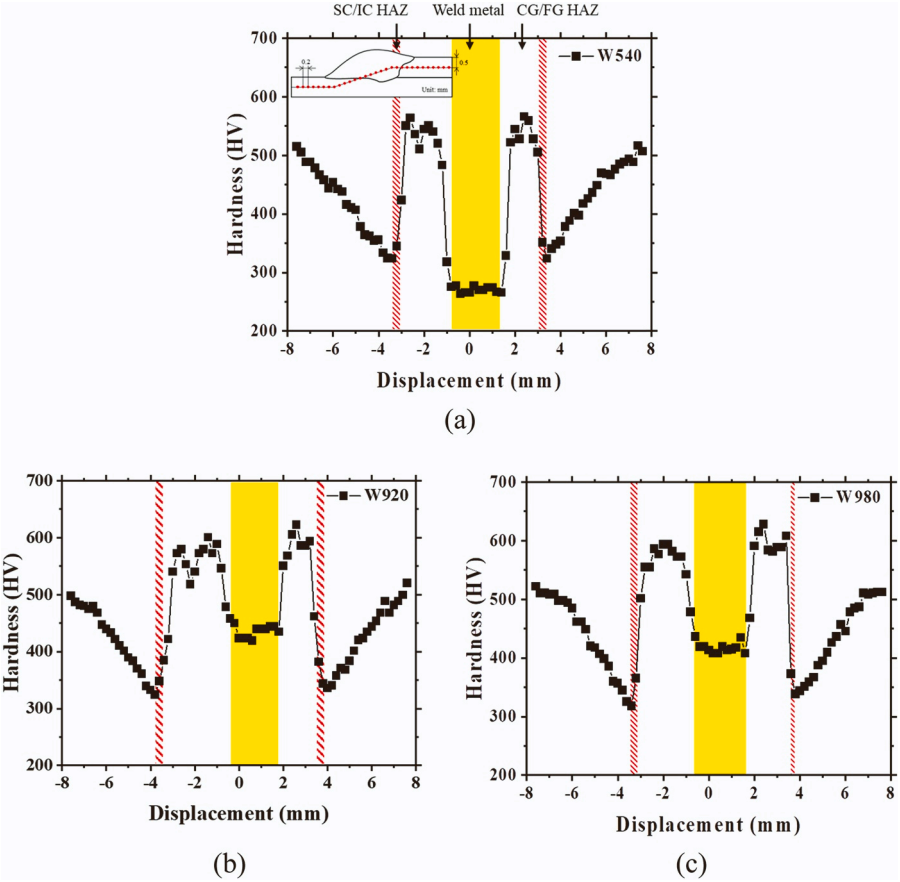

Fig. 10. Measured hardness according to each wire (WFS: 7.0 m/min): **a)** W540, **b)** W920, and **c)** W980. The yellow and red zones represent the WM and ICHAZ, respectively.

attributes, the throat thickness had a strong linear relationship with the joint strength.

3. Under low WFS, that is, when the welding current was low, the high strength filler wire increased the joint strength. However, the conventional low strength filler wire, W540, was applied by using the penetration enhanced modes, such as the standard and pulse model.

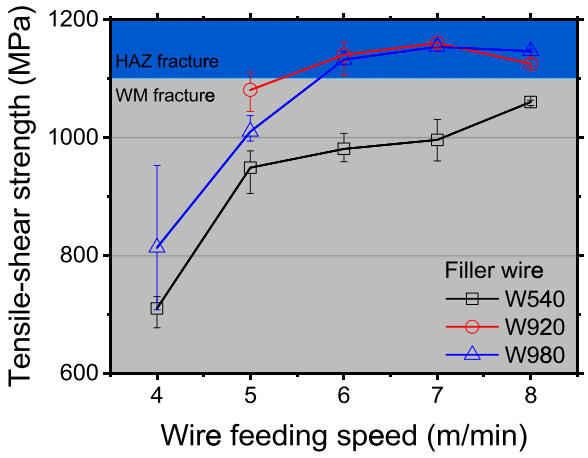

Fig. 11. Equivalent tensile stress corresponding to the measured fracture load at the tensile-shear test.

Further, in high WFS regions, W540 had a slightly smaller strength than W920 and W980.

In this study, the tensile-shear strength and microstructure for the lap joint welding of HPF 2.0 steel sheets were provided for undermatched filler metals. Further studies will include the fatigue characteristic and design rule for the throat thickness while considering the chemical composition of WM and BM.

CRediT authorship contribution statement

Dong-Yoon Kim: Investigation, Analysis, Writing – original draft. **Tae Hyen Lee:** Welding experiment, Data curation. **Cheolhee Kim:** Conceptualization, Methodology. **Minjung Kang:** Visualization, Writing – original draft, Writing – review & editing, Funding acquisition. **Junhong Park:** Supervisor.

Declaration of Competing Interest

The authors declare that they have no known competing financial interests or personal relationships that could have appeared to influence the work reported in this paper.

Data Availability

No data was used for the research described in the article.

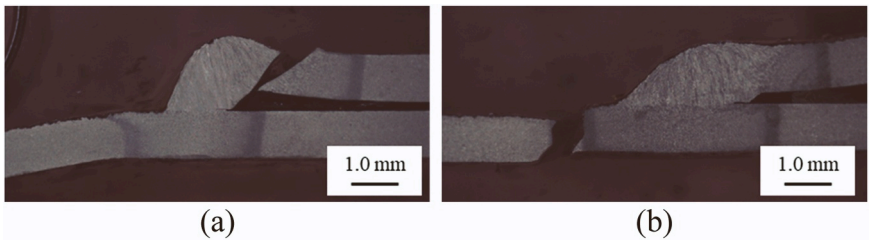

Fig. 12. Fractured specimens after tensile-shear test: **a)** WM fracture (W920, WFS: 5.0 m/min) and **b** HAZ fracture (W920, WFS: 7.0 m/min).

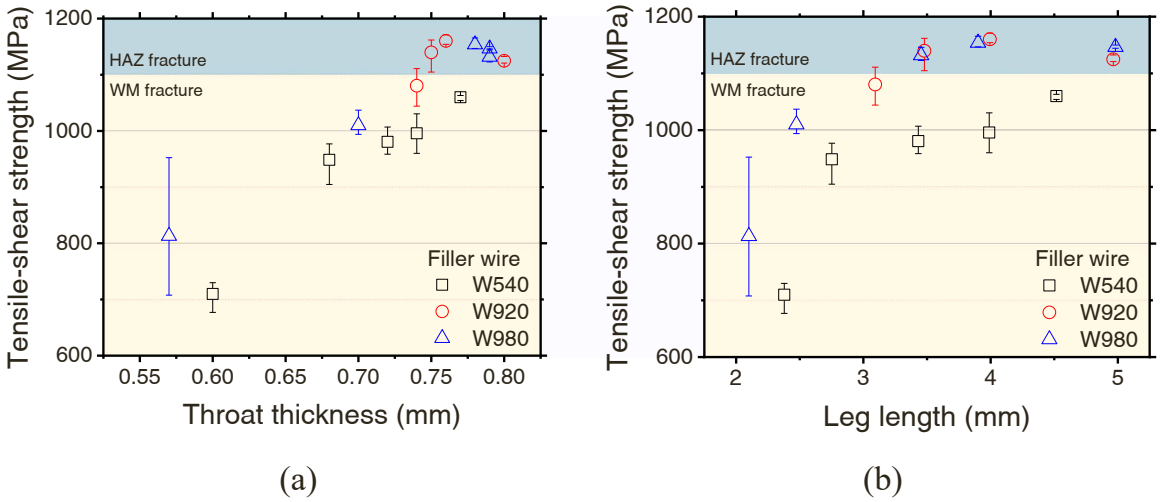

Fig. 13. Tensile-shear strength regarding a) throat thickness and b) leg length.

Acknowledgment

We acknowledge the financial & technical support provided by the Korea Institute of Industrial Technology, South Korea (grant ID: EH-22-060)

References

[1] Z. Zhang, X. Wang, Q. Sun, B. Yang, L. Xiong, H. Liu, Study on microstructure and properties of laser dissimilar welded joints of ultra-high strength PHS1500/PHS2000 steel, Opt. Laser Technol. 150 (2022), 107933, https://doi.org/10.1016/j.optlastec.2022.107933.

[2] L. Lu, Z. Liang, J. Yang, Q. Sun, T. Zhu, X. Wang, Investigation on laser welding of a novel hot-stamped steel with 2000 MPa, J. Mater. Res. Technol. 9 (6) (2020) 13147–13152, https://doi.org/10.1016/j.jmrt.2020.09.044.

[3] W.S. Du, Y. Peng, H.J. Xiao, C.H. He, Z.L. Tian, Microstructure and toughness of 1000 MPa high strength weld metal, in, Mater. Sci. Forum 638 (2010) 3441–3446, https://doi.org/10.4028/www.scientific.net/MSF.638-642.3441.

[4] P. Haslberger, W. Ernst, R. Schnitzer, High resolution imaging of martensitic all-weld metal, Sci. Technol. Weld. Join. 22 (4) (2017) 336–342, https://doi.org/10.1080/13621718.2016.1240980.

[5] E. Keehan, J. Zachrisson, L. Karlsson, Influence of cooling rate on microstructure and properties of high strength steel weld metal, Sci. Technol. Weld. Join. 15 (3) (2010) 233–238, https://doi.org/10.1179/136217110×12665048207692.

[6] K. Kim, N. Kang, M. Kang, C. Kim, Assessment of heat-affected zone softening of hot-press-formed steel over 2.0 GPa tensile strength with bead-on-plate laser welding, Appl. Sci. 11 (13) (2021) 5774, https://doi.org/10.3390/app11135774.

[7] Y. Lu, A. Peer, T. Abke, M. Kimchi, W. Zhang, Subcritical heat affected zone softening in hot-stamped boron steel during resistance spot welding, Mater. Des. 155 (2018) 170–184, https://doi.org/10.1016/j.matdes.2018.05.067.

[8] M. John, P.A. Kumar, K.U. Bhat, P.D. Bhat, A study on HAZ behaviour in 800 MPa cold rolled and hot rolled steel weld, Mater. Today Proc. 44 (2021) 2985–2992, https://doi.org/10.1016/j.matpr.2021.02.124.

[9] M. Tümer, F. Pixner, R. Vallant, J. Domitner, N. Enzinger, Mechanical and microstructural properties of S1100 UHSS welds obtained by EBW and MAG welding, Weld. World 66 (6) (2022) 1199–1211, https://doi.org/10.1007/s40194-022-01276-7.

[10] X. Wang, Y. Wu, H. Pan, C. Yao, J. Huang, Microstructure and softening of advanced high-strength steel QP1180 lap joints welded with CMT, Mater. Lett. 287 (2021), 129282, https://doi.org/10.1016/j.matlet.2020.129282.

[11] T. Zhu, H. Liu, X. Wang, Y. Chen, Y. Wang, Y. Hu, B. Yang, W. Chen, Effect of welding current on microstructure and properties of 2 GPa press-hardened steel joints by RSW, Mater. Res. Express 6 (11) (2019) 1165h5, https://doi.org/10.1088/2053-1591/ab506e.

[12] K. Kim, N. Kang, M. Kang, C. Kim, Effect of laser beam wobbling on the overlap joint strength of hot-press-forming steel over 2.0 GPa tensile strength, J. Laser Appl. 34 (2022), 012012, https://doi.org/10.2351/7.0000447.

[13] M. Kang, Y. Kwak, H. You, S. Kang, C. Kim, Overlap welded joint strength of 2.0 GPa-strength steel sheets using single-mode laser wobbling, J. Laser Appl. 34 (4) (2022), 042013, https://doi.org/10.2351/7.0000730.

[14] M. John, P.A. Kumar, K.U. Bhat, Effect of filler wire strength on high strength low alloy steels, Mater. Today Proc. 49 (2022) 1286–1293, https://doi.org/10.1016/j.matpr.2021.06.376.

[15] C. Chovet, S. Guiheux, Possibilities offered by MIG and TIG brazing of galvanized ultra high strength steels for automotive applications, Metall. Ital. 98 (7) (2006) 47–54.

[16] M. Khurshid, Z. Barsoum, N.A. Mumtaz, Ultimate strength and failure modes for fillet welds in high strength steels, Mater. Des. 40 (2012) 36–42, https://doi.org/10.1016/j.matdes.2012.03.048.

[17] A. Umekuni, K. Masubuchi, Usefulness of undermatched welds for high-strength steels, Weld. J. 76 (7) (1997) 256–263.

[18] P. Haslberger, S. Holly, W. Ernst, R. Schnitzer, Microstructure and mechanical properties of high-strength steel welding consumables with a minimum yield strength of 1100 MPa, J. Mater. Sci. 53 (9) (2018) 6968–6979, https://doi.org/10.1007/s10853-018-2042-9.

[19] T. Björk, A. Ahola, N. Tuominen, On the design of fillet welds made of ultra-high-strength steel, Weld. World 62 (5) (2018) 985–995, https://doi.org/10.1007/s40194-018-0624-4.

[20] I. Hwang, H. Yun, D. Kim, M. Kang, Y.M. Kim, Gas metal arc weldability of 1.5 GPa grade martensitic steels, Met. Mater. Int. 24 (1) (2018) 149–156, https://doi.org/10.1007/s12540-017-7188-5.

[21] K. Kim, H. Park, N. Kang, S. Kang, M. Kang, C. Kim, Mechanical and microstructural properties of autogenous arc welds of 2 GPa-strength hot-press-forming steel, 2022. ⟨https://doi.org/10.21203/rs.3.rs-2130179/v1⟩ (Preprint).

[22] K. Kim, N. Kang, M. Kang, C. Kim, Assessment of heat-affected zone softening of hot-press-formed steel over 2.0 GPa tensile strength with bead-on-plate laser welding, Appl. Sci. 11 (13) (2021) 5774, https://doi.org/10.3390/app11135774.

[23] M. Chen, D. Zhang, C. Wu, Current waveform effects on CMT welding of mild steel, J. Mater. Process. Technol. 243 (2017) 395–404, https://doi.org/10.1016/j.jmatprotec.2017.01.004.
[24] SSAB, Press hardening steels (PHS) for complex shapes. ⟨https://www.ssab.com/en/brands-and-products/docol/automotive-steel-grades/press-hardening-steel⟩ (Accessed 27 November 2022).
[25] K. Kim, N. Kang, M. Kang, C. Kim, Effect of laser beam wobbling on the overlap joint strength of hot-press-forming steel over 2.0 GPa tensile strength, J. Laser Appl. 34 (1) (2022), 012012, https://doi.org/10.2351/7.0000447.
[26] C.A. Apple, G. Krauss, The effect of heating rate on the martensite to austenite transformation in Fe-Ni-C alloys, Acta Metall. 20 (7) (1972) 849–856, https://doi.org/10.1016/0001-6160(72)90077-6.
[27] S. Rhee, E. Kannatey-Asibu, Observation of metal transfer during gas metal arc welding, Weld. J. 71 (1992) 381–386.
[28] D. Srinivasan, P. Sevvel, I.J. Solomon, P. Tanushkumaar, A review on Cold Metal Transfer (CMT) technology of welding, Mater. Today: Proc. 64 (1) (2022) 108–115, https://doi.org/10.1016/j.matpr.2022.04.016.